Article

Biomechanical design of intelligent flexible pulse monitoring system based on biosensors

Ping Li

School of Electrical and Computer Engineering; Nanfang College, Guangzhou 510970, China; lipcat2008@outlook.com

Abstract: As the biosensor technology rapidly develops, the application of flexible sensors in health monitoring is receiving increasing attention. To achieve high-precision, non-invasive, and continuous blood pressure monitoring, a flexible pulse biosensor based on modified multi-walled carbon nanotubes is studied, designed, and prepared. The sensor adopts a dual conductive layer resistive structure and combines crack structure design to enhance the sensitivity and response speed of the sensor. This design fully considers the biomechanical properties to ensure that the sensor can adapt to the strain changes caused by human movement, thereby improving the accuracy and reliability of monitoring. In addition, the study combines time-frequency analysis methods with fast Fourier transform to extract key feature points of pulse signals and uses a BPNN model to predict current blood pressure values. The results show that within a small strain range, the response time of the sensor is only 56.14 ms, and the strain coefficient is as high as 1572.4, effectively achieving real-time monitoring. This high response speed and sensitivity enable the sensor to accurately capture changes in pulse waveforms related to biomechanics, providing more reliable data support. The error of the average arterial pressure obtained by the prediction model is only −0.070 mmHg, which proves the accuracy of the current blood pressure value prediction. In summary, the intelligent flexible pulse monitoring system based on biosensors studied can achieve high-precision real-time blood pressure measurement and has good stability and anti-interference ability, providing effective technical support for home health management and early monitoring of hypertension. This research not only promotes the development of biosensor technology but also provides a new research direction in the field of biomechanics.

Keywords: Internet of Things; biosensors; pulse monitoring; remote medical diagnosis

1. Introduction

As the national living standards improve, people's health awareness is also constantly increasing. In addition, with the arrival of an aging society, health management and disease prevention have become hot topics in modern society. Hypertension, as a common and dangerous chronic disease, has become a major public health challenge worldwide [1]. Based on the World Health Organization (WHO) report, hypertension is a major risk factor for various fatal diseases such as cardiovascular disease and stroke [2]. The pulse of the human body contains rich cardiovascular physiological and pathological information. Therefore, monitoring the pulse waveform to obtain cardiovascular characteristic information plays a critical part in the early detection and prevention of hypertension. This is particularly important as early intervention can significantly reduce the risks associated with high blood pressure, including heart attacks and strokes, which are prevalent in the aging population. Pulse, as a common physiological signal, can provide medical information related to cardiovascular health through its waveform [3]. Compared with traditional

blood pressure monitoring methods that suffer from measurement discontinuity, cumbersome operation, and poor comfort, biosensors have the characteristics of being lightweight, wearable, comfortable, and well attached to the surface of the human body. This adaptability makes biosensors particularly suitable for continuous monitoring in everyday settings, allowing individuals to track their health without the need for frequent clinical visits. They can provide users with continuous, non-invasive, and high-precision physiological signal monitoring [4]. Wang et al. developed a wearable, multi-channel pulse state monitoring system grounded on flexible pressure sensors, thereby confirming the system's capacity to measure pulse signals of varying individuals in different situations [5]. This versatility is crucial, as it indicates that such systems can cater to diverse populations, including those with different health conditions and lifestyles. Venugopal et al. discussed the design field of different blood pressure sensors and confirmed the effectiveness of biosensors in pulse measurement [6]. Therefore, in this context, innovative research is being conducted on the use of biosensors for the design of intelligent flexible pulse monitoring systems, and flexible sensors are prepared using modified multi-walled carbon nanotubes (MWCNTs). These materials are chosen for their exceptional electrical conductivity and mechanical flexibility, making them ideal for creating sensors that can conform to the body's contours while maintaining high performance. At the same time, a dual conductive layer resistive structure combined with a crack structure design is used to raise the sensitivity and response speed of the sensors. This innovative design approach not only enhances the sensor's performance but also ensures that it can accurately capture subtle changes in pulse characteristics, which are vital for effective hypertension monitoring. This study investigates an intelligent, flexible pulse monitoring system grounded on biosensors with a view to improving real-time blood pressure monitoring accuracy and providing effective technical support for family health management and early screening of hypertension.

2. Design of cardiovascular health monitoring system based on biological FPS

2.1. Design and preparation of FPS monitoring system

With the rapid development of high-tech such as artificial intelligence, 5G, and others, various intelligent devices are entering people's daily lives in unprecedented forms, profoundly changing their way of life [7]. Therefore, wearable devices based on biosensors have become a new data traffic portal in the mobile Internet era, gradually making people feel the convenience and charm brought by technology [8]. As the core component of cardiovascular health monitoring systems, sensors need to be designed to balance high sensitivity and good stability to ensure accurate capture of pulse signals [9]. Besides, the selection of materials is crucial to ensure the comfort and durability of sensors during long-term wear. Therefore, the study chose waterborne polyurethane (WPU) with high conductivity and flexibility as the substrate material for the sensor. WPU is a polyurethane material dispersed in water, mainly composed of polyols, isocyanates, and chain extenders [10]. It not only has good biocompatibility but also has the advantages of being environmentally friendly, safe,

and easy to process and modify, making it very suitable as a material for long-term skin contact. Therefore, WPU was chosen as the substrate material for the sensor, possessing ideal flexibility to adapt to complex deformations and movements on the skin surface. The preparation of the flexible pulse sensor (FPS) is denoted in **Figure 1**.
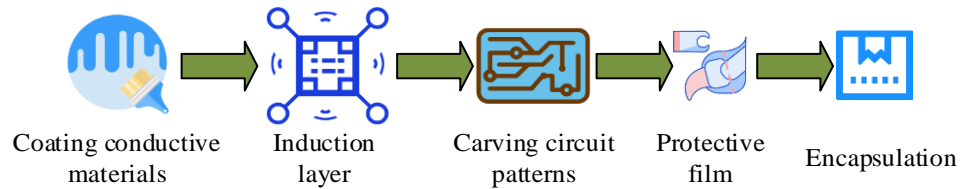

Figure 1. Preparation process of FPS.

In **Figure 1**, in the preparation of the FPS, the conductive material is first uniformly coated on the WPU substrate to form the sensing layer. At this point, the thickness of the conductive coating is controlled at 25 microns to ensure the sensitivity and response speed of the sensor. At the same time, laser etching technology is used to finely carve the circuit pattern of the sensor. The wavelength of the laser is 355 nm, the power is set to 50 mW, and the etching speed is 5 mm/s. By controlling the density and speed of the laser scanning, the precision of the circuit pattern is optimized to ensure high sensitivity and resolution. To raise the signal-to-noise ratio and anti-interference ability of the sensor, a protective film with a thickness of 5 microns is on the surface of the sensor to enhance its durability and stability. Finally, the sensor was integrated into wearable devices through packaging technology, enabling real-time monitoring of the user's pulse waveform and providing continuous and accurate cardiovascular health data support. In the selection of conductive materials, MWCNTs were chosen for the study. To improve the dispersibility and conductivity of MWCNTs, a chemical modification treatment was first carried out during the preparation process.

In the preparation process of modified MWCNTs, 0.5 g of MWCNTs material was first weighed and subjected to magnetic stirring to ensure uniform dispersion in the solvent. Next, 5 mL of dimethylformamide (DMF) was added to the solvent to further assist in the dispersion of carbon nanotubes and provide a suitable environment for subsequent chemical reactions. Next, the solution was placed in an ultrasonic signal generator for 30 min of high-frequency ultrasonic oscillation to prevent the aggregation of carbon nanotubes in the solution. Then, during the slow stirring of the solvent, 45 mL of thionyl chloride ($SOCl_2$) was slowly added to introduce chloride groups [11]. Subsequently, the solvent was heated and refluxed to react with the surface of the carbon nanotubes to ensure sufficient chlorination reaction. Finally, the modified MWCNTs solid could be recovered by allowing the mixed solution to cool to room temperature. In the coating process of conductive materials, to raise the sensitivity and response speed of sensors, a double conductive layer resistive structure was adopted to make the electric field distribution more uniform. Besides, the study also uses crack design to further raise the sensitivity of flexible sensors. The inspiration for the crack structure comes from the narrow, slit-shaped sensory organs of arthropods such as spiders and scorpions, which can sense small mechanical stress

changes when subjected to external forces. The sensor mechanism based on the double conductive layer crack structure is denoted in **Figure 2**.
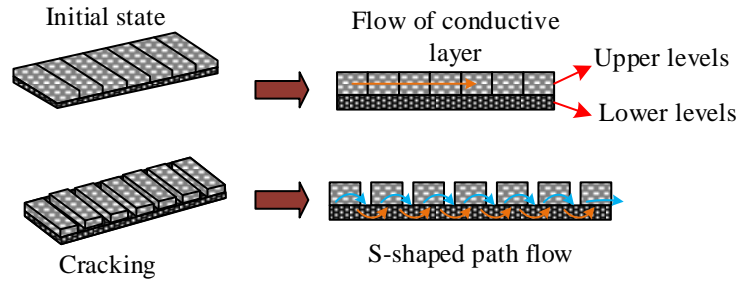

Figure 2. Sensor mechanism based on double conductive layer crack structure.

In **Figure 2**, in the initial state, the crack gap of the sensor can be almost ignored, and the current mainly flows through the upper conductive layer. When cracks change under pressure from the outside, the path for electricity forms an S-shaped path. This structure ensures that even under high strain, the conductive path remains unobstructed [12]. In addition, cracks can cause significant changes in resistance during the cracking and closing process, thereby improving the response speed and sensitivity of sensors. The calculation for sensor sensitivity is denoted in Equation (1).

$$SE = \frac{R - R_0}{\varepsilon R_0} = \frac{n \Delta R}{\varepsilon R_0} \tag{1}$$

In Equation (1), SE represents sensitivity, R represents sensor resistance, R_0 represents initial resistance, ε represents strain, n means the amount of cracks, and ΔR means the increased resistance of the lower conductive layer. The resistance of the lower conductive layer is shown in Equation (2).

$$R_2 = n \Delta R + R_1 \tag{2}$$

In Equation (2), R_2 and R_1 represent the resistance of the lower and upper conductive layers, respectively [13].

2.2. Blood pressure prediction model based on improved BPNN

On the basis of the design and preparation of FPSs, one of the core tasks of cardiovascular health monitoring systems is to accurately predict blood pressure values. Therefore, the study is based on signal data obtained from FPSs and utilizes neural network structures for blood pressure prediction (BPP) and analysis. Backpropagation neural network (BPNN) can optimize network parameters through the backpropagation algorithm [14]. Its multi-layer structure design has feedback and memory functions and can handle high-dimensional and nonlinear data, thus exhibiting excellent performance in complex data prediction [15]. Therefore, the construction of a BPP model based on BPNN is studied. BPNNs are typically comprised of three layers: an inputting layer, a hidden layer (HL), and an outputting layer. The function of the HL is to enhance the predictive ability of the model [16]. The study extracts effective features from signals collected by FPSs, normalizes them, and sends them as input data to the BPNN for training. By continuously adjusting weights and biases in the network to minimize prediction errors, the accuracy of BPP

can be improved. The specific formula for the forward propagation process is shown in Equation (3).

$$H_j = \sigma \times \left(\sum_{i=1}^{m} I_i \times \omega_{ij} + b_j^H \right), j = 1, 2, \ldots, k \qquad (3)$$

In Equation (3), H_j denotes the output of the j-th neuron in the HL, k denotes the amount of neurons in the HL, σ means the activation function, I_i denotes the input value of the i-th feature in the input layer, m indicates the total amount of features in the input layer, ω_{ij} refers to the weight between the i-th feature and the j-th neuron in the inputting layer, and b_j^H denotes the bias of the j-th neuron in the HL [17]. The calculation formula for the loss function is denoted in Equation (4).

$$L = \frac{1}{2} \sum_{a=1}^{r} e_a^2 \qquad (4)$$

In Equation (4), L represents the loss function, r denotes the amount of output layer neurons, and e_a represents the error of the a-th output neuron. The study uses the gradient descent method for weight adjustment, and the update amount of weight adjustment is shown in Equation (5).

$$\Delta \omega_{ja}(t) = -\frac{\eta \times \partial L(t)}{\partial \omega_{ja}(t)} \qquad (5)$$

In Equation (5), $\Delta \omega_{ja}(t)$ denotes the update amount of weights in the t-th iteration, j and a represents the neurons in the HL and outputting layer, η represents the learning rate, and ∂ represents the partial derivative [18]. The update amount of bias adjustment is shown in Equation (6).

$$\Delta b_a(t) = -\frac{\eta \times \partial L(t)}{\partial b_a(t)} \qquad (6)$$

In Equation (6), $\Delta b_a(t)$ represents the update amount of bias in the t-th iteration. However, although the HL structure of BPNNs increases the expressive power of the model, it may also lead to slower training speed and cause overfitting. To address this issue, a genetic algorithm was used to improve the BPNN and construct a BPP model based on the improved BPNN. The workflow of this model is denoted in **Figure 3**.
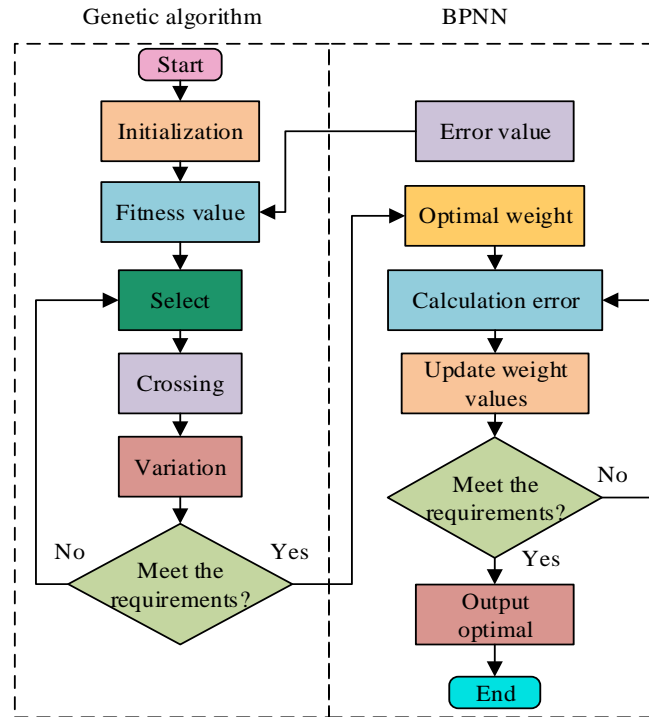
Figure 3. Process of BPP model based on improved BPNN.

In **Figure 3**, in the improved BPNN process, the error value is first trained using the BPNN and input as the fitness value into the genetic algorithm. Next, genetic algorithms optimize fitness values through operations such as selection, crossover, and mutation. For the optimized fitness values, it is determined whether the set threshold requirements are met. If the conditions are met, it will be input into the BPNN for optimal weight calculation. If the conditions are not met, it will return to the previous layer of the genetic algorithm and perform operations such as selection, crossover, and mutation again. After calculating the optimal weights, BPNN is used for error calculation, and the weights are updated based on the error. Finally, it is necessary to judge whether the updated weights satisfy the conditions. If it is satisfied, the optimal weights are output, and the process ends; otherwise, it will continue to recalculate the errors and adjust the weights until the requirements are satisfied. The key parameters of the genetic algorithm optimization process include population size and iteration times. In the study, the population size of the genetic algorithm was set to 50, and the number of iterations was set to 100. These parameters play an important role in the optimization process, ensuring the algorithm's global search capability and convergence speed. Among them, the population size determines the number of candidate solutions involved in optimization in each iteration, and the number of iterations determines the optimization depth of the algorithm. By introducing genetic a algorithm to optimize BPNN, research can effectively avoid overfitting caused by overly complex network structures, thereby achieving real-time blood pressure change prediction of pulse data while ensuring prediction accuracy. The calculation for the fitness function is denoted in Equation (7).

$$F = \frac{2}{\sum_{a=1}^{r}(D_{out} - A_{out})} \tag{7}$$

In Equation (7), F represents the fitness function value, and D_{out} and A_{out} respectively represent the expected output and actual output results of the BPNN structure. The probability of selecting the genetic operator is shown in Equation (8).

$$P = \frac{f(\alpha)}{\sum_{\alpha=0}^{u} f(\alpha)} \tag{8}$$

In Equation (8), P denotes the probability of selecting the genetic operator, α means the fitness value of the genetic operator, $f(\alpha)$ represents the area occupied by the selected genetic operator in all individuals, and u means the total amount of genetic operators. The monitoring system design is shown in **Figure 4**.
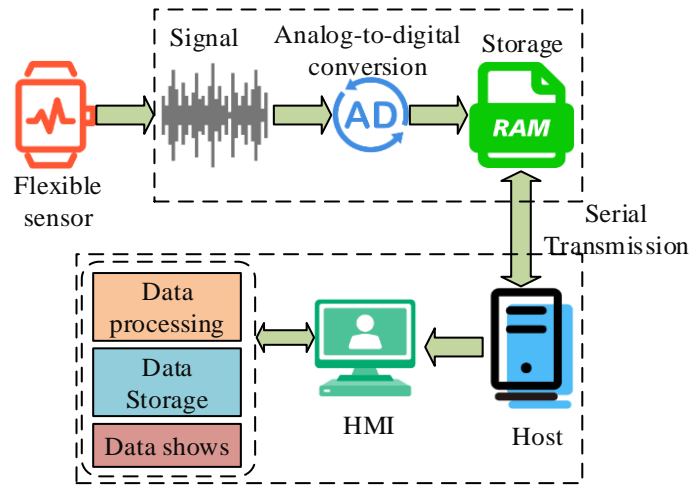

Figure 4. Monitoring system design.

In **Figure 4**, the designed monitoring system collects electronic signals through flexible sensors, which are stored in random access memory after analog-to-digital conversion. Subsequently, the signal is transmitted serially through the serial bus interface and transmitted to the upper computer through the serial bus communication module. Finally, the upper computer processes, stores, and displays the data.

3. Verification of cardiovascular health monitoring system based on flexible pulse biosensor

3.1. Experimental environment setup

To assess the effectiveness of the cardiovascular health monitoring system based on flexible pulse biosensors, an experimental environment for static and dynamic characteristic testing was established. In a static testing environment, real-time data analysis was conducted through a data acquisition computer, data acquisition was carried out using a data acquisition card, and external strain force was provided through a tensile and compressive testing machine. At the same time, a DC resistance tester was used to test the resistance changes of sensors. The dynamic testing environment added a signal generator to generate electrical signal excitation on the basis of static testing and used a test box vibration platform to simulate pulse vibration. To ensure good representativeness of the experimental results, a total of 10 sensor samples were used for static testing. Each sensor sample is measured under external

strain ranging from 0 to 100%, ensuring that the measurement data covers the working range of the sensor. The resistance change data of all sensors is transmitted and analyzed in real-time through a data acquisition card to ensure high-precision data collection and processing. After collecting the data, all signal data is first preprocessed through filtering and denoising operations to improve the accuracy of analysis. Then, the 10-fold cross-validation method is used to train the data, with the input of the model being the time-frequency characteristics of the pulse signal and the output being the corresponding blood pressure value. The experimental environment configuration is denoted in **Table 1**.

Table 1. Experimental environment configuration.

Equipment name	Specification	Purpose
Data Acquisition Card	NI USB-6211	Used for data acquisition
Tensile and Compression Testing Machine	TH2515	Provides external strain force for testing
DC Resistance Tester	TH2515	Measures the resistance change of the sensor
Signal Generator	Agilent 33220A	Generates electrical signal excitation
Vibration Platform	LK-2003A	Simulates pulse vibration

3.2. Performance verification of FPS

To verify the effectiveness of the FPS, the sensitivity coefficients of the designed dual conductive layer crack structure sensor (DCLCSS), single-layer sensor structure, and double-layer crack-free sensor structure were compared and studied. The sensitivity coefficient comparison of different sensor designs is denoted in **Figure 5**. From **Figure 5a**, in the static characteristic test, when the tensile strain was only 2%, the single-layer sensor structure was prone to fracture, and its maximum sensitivity coefficient was 3×10^2. However, the two double-layer structures did not show a trend of fracture with the increase of tensile strain, and the sensitivity coefficient gradually increased with the increase of strain. The maximum sensitivity coefficients of the DCLCSS and the double-layer crack-free structure studied reached 1×10^3 and 5×10^2, respectively. From **Figure 5b**, in the dynamic characteristic test, the maximum sensitivity coefficient of the double conductive layer crack structure sensor studied is 1.1×10^3, while the maximum sensitivity coefficients of the single-layer sensor structure and the double-layer crack-free sensor structure are 4×10^2 and 8×10^2, respectively. In summary, the DCLCSS exhibits higher sensitivity coefficients in both static and dynamic tests, verifying its superior performance.
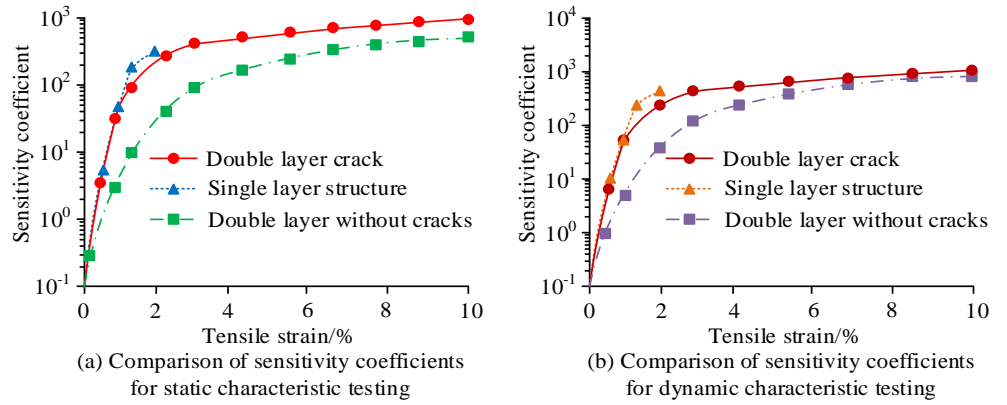
(a) Comparison of sensitivity coefficients for static characteristic testing

(b) Comparison of sensitivity coefficients for dynamic characteristic testing

Figure 5. Sensitivity coefficient comparison of different sensor designs.

The dynamic response performance of the FPS is denoted in **Figure 6**. From **Figure 6a**, under both high and low strain testing environments, the resistance of the sensor steadily increased, indicating that the sensor can stably capture dynamic signals. In the large strain range, the maximum response time of the sensor was only 41.25 ms, while in the small strain range, the response time was only 56.14 ms, indicating that the sensor has excellent sensitivity. From **Figure 6b**, during the stress loading and unloading process of the sensor, the strain coefficient gradually increased with the increase of strain. When the stress reached the maximum value of 10%, the maximum strain coefficient generated was 1572.4. In addition, the strain coefficient changes during the loading and unloading processes exhibited a high degree of symmetry, indicating that under the same loading and unloading strain conditions, the resistance changes are relatively small, further verifying that the sensor has good recovery performance.
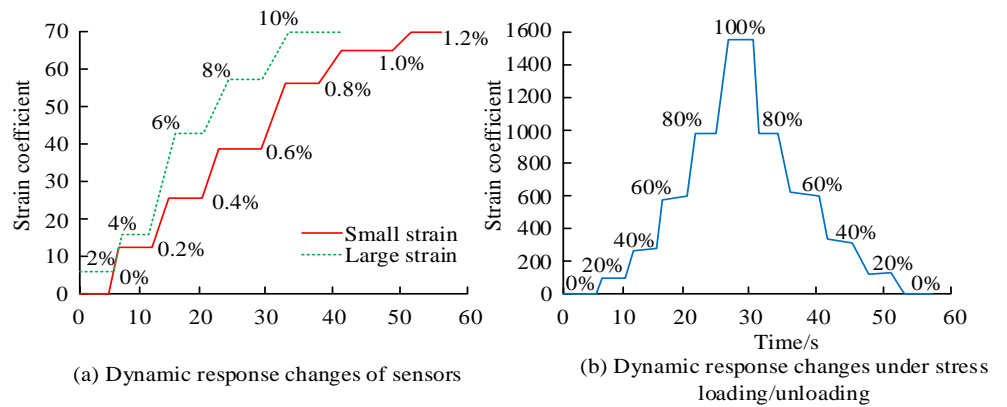

(a) Dynamic response changes of sensors

(b) Dynamic response changes under stress loading/unloading

Figure 6. Dynamic response performance of FPS.

To prove the effectiveness of FPSs in practical applications, a study was conducted by wearing the sensor on the wrist and using repetitive movements of the wrist to verify the response effect of the sensor. The sensor response results for different wrist movements are shown in **Figure 7**. From **Figure 7a**, during wrist flexion and extension movements, the sensor resistance exhibited a regular, repetitive response with changes in movement. The resistance during wrist bending and extension was 110 Ω and 100 Ω, respectively. This is because when the wrist bent, the sensor resistance gradually increased, and when the wrist returned to its original state

or extended, the resistance gradually decreased. From **Figure 7b**, under wrist rotation, the sensor resistance changed in a stepwise pattern with the rotation angle. When the wrist's rotation angle was 90 degrees, the resistance reached its maximum value of 110 Ω. In summary, the sensors studied can still maintain excellent monitoring sensitivity and stability during wrist movements. The sensor used in the study is a crack structure, which undergoes deformation under external stress, especially when the contact pressure changes. The opening and closing of the crack can adjust the current path and maintain smooth conductivity. Therefore, sensors can dynamically adapt to pressure changes when in contact with the skin, reducing signal fluctuations caused by uneven pressure distribution or poor adhesion. In addition, cracks can cause significant changes in resistance during the cracking and closing process. This means that even if the sensor makes small changes in contact with the skin, such as skin surface deformation, pressure changes, etc., the crack structure can effectively amplify these changes and provide a more sensitive response.
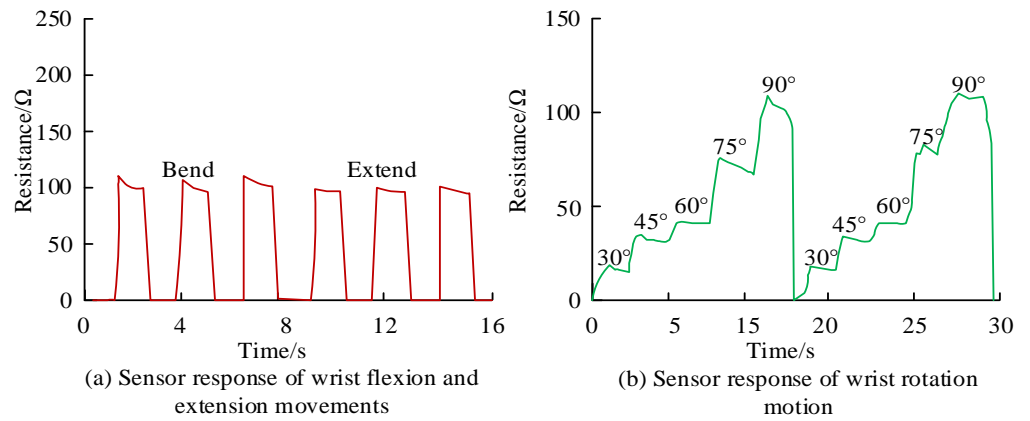

(a) Sensor response of wrist flexion and extension movements

(b) Sensor response of wrist rotation motion

Figure 7. Sensor response results of different wrist movements.

3.3. Performance verification of BPP model based on improved BPNN

To prove the effect of the BPP system, the study collected the system's effectiveness in practical use, and the findings are denoted in **Table 2**. In **Table 2**, the data acquisition error of the monitoring system was controlled within ± 3 mmHg, indicating a high accuracy of data acquisition. The response time of the entire system process was about 0.2 s, and in actual operation testing, the response of the user interface was smooth, with an operation time of less than 1 s, reflecting the high fluency of the system. In addition, during the long-term running test, the system did not experience any crashes, indicating its high stability.

Table 2. System performance results.

Verification item	Verification method	Result	Remarks
Data acquisition accuracy	Blood pressure sensor test	Error ≤ ±3 mmHg	Sensor performance is good
System response time	Full system process test	Approximately 0.2 s	Includes data acquisition and prediction process
System stability	Long-term operation test	No crashes	The system operates stably
User interface response	Actual operation test	Response time < 1 s	The user interface is smooth

To validate the effect of the BPP model grounded on the improved BPNN, the pulse signals collected by the FPS were preprocessed and broken into training and testing sets in a 3:7 ratio. Then, the study compared and analyzed the improved BPNN prediction model with other advanced prediction models. Other models included traditional BPNN models, long short term memory (LSTM) network models, and random forest (RF) models [19,20]. In all experiments, the improved BP neural network model used the same hyperparameter settings and cross-validation strategy as the traditional BP neural network model, LSTM network model, and RF model. All models were trained with a learning rate of 0.001, two hidden layers, 10 nodes per layer, and 50 rounds of training. In addition, in order to reduce overfitting issues during model training, all models underwent 5-fold cross-validation to ensure the reliability and universality of the results. The comparison of mean arterial pressure errors between different prediction models is denoted in **Figure 8**. From **Figure 8a**, in the training set, the average arterial pressure error of the research model was only −0.080 mmHg, while the average errors of the traditional BPNN model, LSTM model, and RF model were −0.120 mmHg, −0.100 mmHg, and −0.110 mmHg, respectively. The average errors of the research model were reduced by 33.33%, 20%, and 27.27%, respectively. The differences reached a statistically significant level ($P < 0.05$). From **Figure 8b**, in the test set, the mean arterial pressure error of the research model was only −0.070 mmHg, while the errors of other models were −0.130 mmHg, −0.120 mmHg, and −0.115 mmHg. The error of the research model on the test set was also relatively small, with reductions of 46.15%, 41.66%, and 39.13%, respectively. The difference is also statistically significant ($P < 0.05$). In summary, the improved BPNN model has low arterial pressure prediction errors in both the training and testing sets, verifying its accuracy and robustness in predicting blood pressure values.
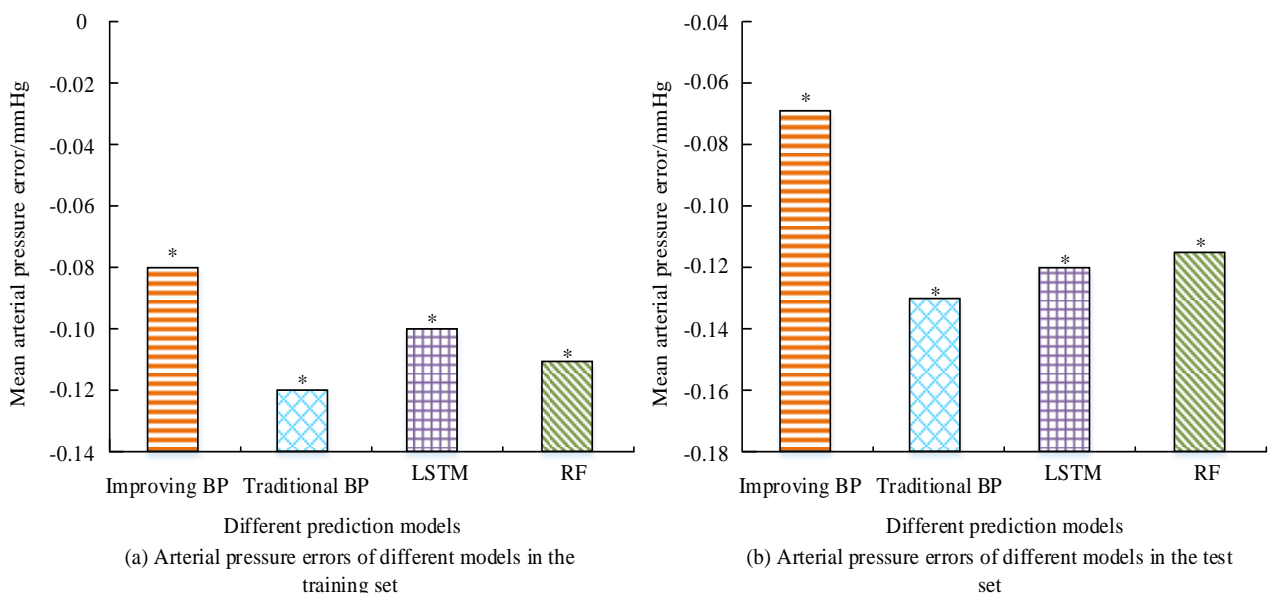

Figure 8. Comparison of mean arterial pressure error between different prediction models.
* indicates $P < 0.05$.

To verify the fitting effect of the blood pressure value prediction model grounded on the improved BPNN, different prediction models were compared and validated

using the same pulse signal. The fitting effect between the predicted values of different models and the true values is shown in **Figure 9**. From **Figure 9a**, the predicted values of systolic and diastolic blood pressure by the research model highly coincided with the expected values, with the maximum error occurring only at the 5th second. At this time, the predicted value of diastolic blood pressure was 75.0 mmHg, the expected value was 73.1 mmHg, and the maximum error was 2.59%. In the fitting effect of the traditional BPNN model in **Figure 9b**, at the 15th second, the predicted value of systolic blood pressure was 105.7 mmHg and the expected value was 112.5 mmHg, with a maximum error of 6.43%. In the fitting effect of the LSTM model in **Figure 9c**, the predicted value of diastolic blood pressure was 56.6 mmHg, the expected value was 66.8 mmHg, and the maximum error was 18.02%. In the fitting effect of the RF model in **Figure 9d**, the predicted value of systolic blood pressure was 105.8 mmHg, the expected value was 113.5 mmHg, and the maximum error was 7.27%. In summary, the BPP model based on the improved BPNN has higher prediction accuracy, lower errors, and better fitting effects compared to other models.

(a) Improving the fitting effect of BP model

(b) The fitting effect of traditional BP model

(c) The fitting effect of LSTM model

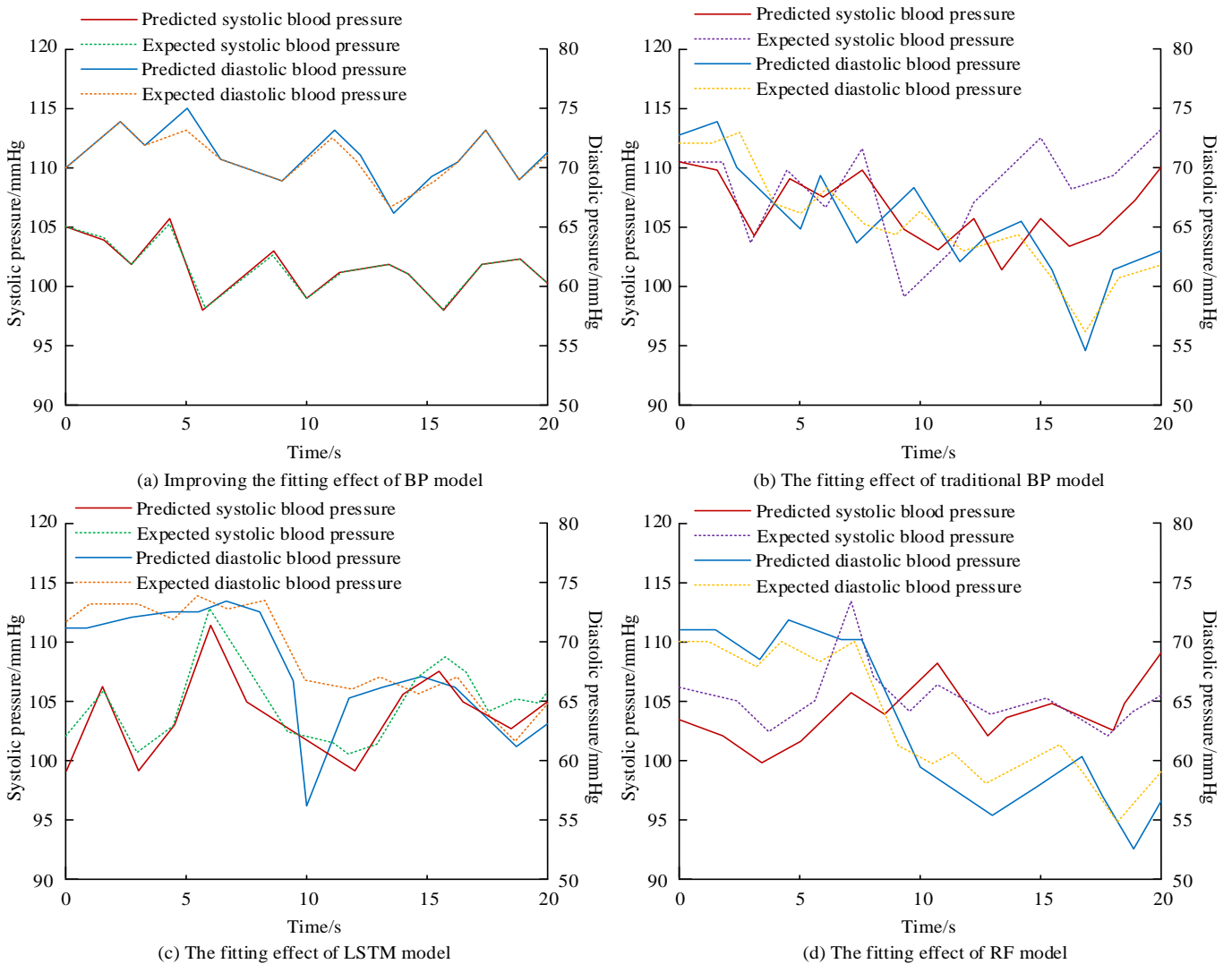(d) The fitting effect of RF model

Figure 9. The fitting effect between predicted values and true values of different models.

To further identify the superiority of the BPP model based on the improved BPNN, the performance of different prediction models was compared and studied, as denoted in **Table 3**. From **Table 3**, the effectiveness of the research model was significantly better than the other three models. On the training set, the mean squared error (MSE) and mean absolute error (MAE) of the research model were both the lowest, at 0.010 and 0.085, respectively, while the MSE and MAE of other models were above 0.10. On the test set, the root mean square error (RMSE) of the research model was the lowest at 0.093, which was reduced by 19.13%, 30.59%, and 25.60% compared to traditional BPNN models, LSTM models, and RF models, respectively. The coefficient of determination R^2 was an important indicator for measuring the fit of a model, and the closer the value was to 1, the better the fit between the model and the data. In the training and testing sets, the R^2 values of the research model were as high as 0.975 and 0.981, while the R^2 values of other models did not exceed 0.95. In terms of prediction accuracy, the research model achieved a prediction accuracy of 93.4% and 94.1% on the training and testing sets, respectively, while the prediction accuracy of other models did not exceed 90%. In summary, the BPP model based on the improved BPNN has strong generalization ability and prediction accuracy.

Table 3. Performance comparison of different prediction models.

Model		MSE	RMSE (mmHg)	MAE (mmHg)	R^2	Prediction accuracy/%
Training set	Improved BPNN	0.010	0.100	0.085	0.975	93.4
	Traditional BPNN	0.016	0.129	0.112	0.945	87.6
	LSTM network	0.023	0.153	0.145	0.925	82.4
	RF	0.018	0.134	0.121	0.940	85.7
Test set	Improved BPNN	0.008	0.093	0.178	0.981	94.1
	Traditional BPNN	0.013	0.115	0.101	0.946	89.3
	LSTM network	0.018	0.134	0.127	0.935	85.7
	RF	0.015	0.125	0.113	0.942	88.2

In order to further verify the superiority of the blood pressure prediction model based on the improved BP neural network, a comparative analysis was conducted with existing commonly used blood pressure monitoring techniques. The performance comparison of different blood pressure monitoring technologies is shown in **Table 4**. From **Table 4**, it can be seen that existing blood pressure monitoring technologies have their own advantages and disadvantages. The cuff-type blood pressure monitor is currently the most common method for measuring blood pressure, but it has limitations such as requiring manual operation, discomfort, and long measurement time. Wrist blood pressure monitors are easily affected by exercise and have unstable accuracy. Although the dynamic blood pressure monitoring system can provide round-the-clock monitoring, the equipment is bulky, inconvenient to wear, and costly. In contrast, the research method can predict blood pressure in real-time while ensuring high accuracy, and the system based on flexible sensors is more comfortable, suitable for long-term wearing, and can adapt to daily activities. Compared to traditional technology, this system has a cost advantage and is particularly suitable for long-term use.

Table 4. Comparison of performance of different blood pressure monitoring technologies.

Technology	Advantage	Disadvantage	Accuracy	Real-time	Comfort
Cuff-type blood pressure monitor	Accurate measurement, widely used in clinical practice	Manual operation is required, and the measurement process is uncomfortable.	Tall	Medium	Differ from
Wrist blood pressure monitor	Easy for household use and relatively low price	Accuracy is easily affected and susceptible to motion interference.	Medium	Faster	Medium
Dynamic blood pressure monitoring system	Provide all-weather blood pressure data, suitable for hypertension diagnosis	The equipment is heavy, inconvenient to wear, and costly.	Tall	Tall	Differ from
Improved BPNN	High precision, real-time prediction, suitable for wearable devices	Requires sensor and algorithm support, relying on pulse signal acquisition.	Tall	Tall	Tall

In order to verify the long-term durability and environmental stability of the sensor, cyclic loading tests and environmental stability tests were conducted. The long-term durability and environmental stability tests of the sensor are shown in **Table 5**. From **Table 5**, it can be seen that in the cyclic loading test, the sensor underwent 10,000 cycles of testing at 50% strain, and the results showed no significant changes in sensitivity and response time. The maximum strain coefficient remained above 1570, demonstrating its durability in long-term use. In the environmental stability test, the sensor underwent a 30-day performance test under different temperature conditions of −20 °C to 60 °C and humidity conditions of 20% to 90%. The results showed that the sensitivity and response time of the sensor under extreme environmental conditions varied within 5%, indicating its good environmental stability. From the above, it can be seen that the sensor not only has excellent performance in the short term but also maintains stability under long-term use and complex environmental conditions, thus verifying the feasibility of the sensor in practical applications.

Table 5. Long-term durability and environmental stability tests of the sensor.

Test type	Test condition	Result	Performance change
Cycle Load Test	50% strain, 10,000 cycles	Sensitivity and response time remained stable.	No significant change
		Maximum strain coefficient remained above 1570.	Stable performance after 10,000 cycles
Environmental Stability Test	Temperature range: −20 °C to 60 °C	Sensitivity and response time changes within 5%.	Stable performance across the temperature range
	Humidity range: 20% to 90%	Sensitivity and response time changes within 5%.	Stable performance across humidity range
	Test duration: 30 days	The sensor performed well in extreme conditions.	Stable performance after 30 days

4. Conclusion

As the social economy continuously develops, people's living standards have significantly improved, and their health awareness is also increasing. To achieve real-time and accurate monitoring of cardiovascular diseases, a non-invasive blood pressure monitoring system was designed using biosensors. The system combined WPU flexible material and MWCNTs conductive material and adopted a double

conductive layer crack structure to design a pulse sensor. It also used an improved BPNN model to predict blood pressure. The outcomes denoted that the sensor achieved sensitivity coefficients of 1×10^3 and 1.1×10^3 in static and dynamic tests, respectively. The response time of the sensor was 41.25 ms in the large strain range and 56.14 ms in the small strain range, indicating its high response speed and sensitivity. When the stress reached the maximum value of 10%, the maximum strain coefficient of the sensor reached 1572.4. In addition, sensors can stably capture dynamic signals during wrist flexion, extension, and rotation movements, demonstrating strong stability and recovery performance in practical applications. In terms of BPP performance, the research model showed high prediction accuracy with prediction errors of −0.080 mmHg and −0.070 mmHg on the training and testing sets. Meanwhile, the R^2 values of the model in the training and testing sets were 0.975 and 0.981, with prediction accuracies of 93.4% and 94.1%, further demonstrating its excellent predictive performance. In summary, the intelligent, flexible pulse monitoring system based on biosensors has high accuracy, stability, and real-time performance in blood pressure monitoring and has broad application prospects. However, despite achieving good experimental results. In current research, the validation process mainly focused on a limited population sample and did not fully consider the potential impact of individual differences such as age, gender, and skin elasticity on the performance of blood pressure monitoring systems. Therefore, although the predictive performance of the research model in the current dataset is good, its universality and reliability in different populations still need further validation. Future research should include extensive testing of different individual characteristics to ensure that the monitoring system can work stably and accurately in diverse populations, further enhancing its clinical reliability and generalizability.

However, current research also has potential limitations and challenges. For example, although sensors perform stably in most static and dynamic environments, their long-term stability still needs further verification, especially the issue of performance degradation after prolonged use. In addition, although the system has good comfort and is suitable for long-term wear, further optimization is still needed for the comfort requirements and adaptability of different individuals. Therefore, future research should consider the challenges in these practical applications and further improve system design to enhance its reliability and wide applicability in complex environments.

Conflict of interest: The author declares no conflict of interest.

References

1. Li L, Liu Y, Song C, et al. Wearable Alignment-Free Microfiber-Based Sensor Chip for Precise Vital Signs Monitoring and Cardiovascular Assessment. Advanced Fiber Materials. 2022; 4(3): 475-486. doi: 10.1007/s42765-021-00121-8
2. Baek S, Lee Y, Baek J, et al. Spatiotemporal Measurement of Arterial Pulse Waves Enabled by Wearable Active-Matrix Pressure Sensor Arrays. ACS Nano. 2021; 16(1): 368-377. doi: 10.1021/acsnano.1c06695
3. Chen G, Au C, Chen J. Textile Triboelectric Nanogenerators for Wearable Pulse Wave Monitoring. Trends in Biotechnology. 2021; 39(10): 1078-1092. doi: 10.1016/j.tibtech.2020.12.011
4. Zhang C, Zhang C, Wu X, et al. An integrated and robust plant pulse monitoring system based on biomimetic wearable sensor. npj Flexible Electronics. 2022; 6(1). doi: 10.1038/s41528-022-00177-5

5. Wang J, Zhu Y, Wu Z, et al. Wearable multichannel pulse condition monitoring system based on flexible pressure sensor arrays. Microsystems & Nanoengineering. 2022; 8(1). doi: 10.1038/s41378-022-00349-3

6. Venugopal K, Panchatcharam P, Chandrasekhar A, et al. Comprehensive Review on Triboelectric Nanogenerator Based Wrist Pulse Measurement: Sensor Fabrication and Diagnosis of Arterial Pressure. ACS Sensors. 2021; 6(5): 1681-1694. doi: 10.1021/acssensors.0c02324

7. Wang Y, Chen P, Zhou X, et al. Highly Sensitive Zwitterionic Hydrogel Sensor for Motion and Pulse Detection with Water Retention, Adhesive, Antifreezing, and Self-Healing Properties. ACS Applied Materials & Interfaces. 2022; 14(41): 47100-47112. doi: 10.1021/acsami.2c14157

8. Ibrahim B, Jafari R. Cuffless blood pressure monitoring from a wristband with calibration-free algorithms for sensing location based on bio-impedance sensor array and autoencoder. Scientific Reports. 2022; 12(1). doi: 10.1038/s41598-021-03612-1

9. Yin YM, Li HY, Xu J, et al. Facile Fabrication of Flexible Pressure Sensor with Programmable Lattice Structure. ACS Applied Materials & Interfaces. 2021; 13(8): 10388-10396. doi: 10.1021/acsami.0c21407

10. Xu D, Ouyang Z, Dong Y, et al. Robust, Breathable and Flexible Smart Textiles as Multifunctional Sensor and Heater for Personal Health Management. Advanced Fiber Materials. 2022; 5(1): 282-295. doi: 10.1007/s42765-022-00221-z

11. Ushakov N, Markvart A, Kulik D, et al. Comparison of Pulse Wave Signal Monitoring Techniques with Different Fiber-Optic Interferometric Sensing Elements. Photonics. 2021; 8(5): 142. doi: 10.3390/photonics8050142

12. Zhang H, Zhang D, Guan J, et al. A flexible wearable strain sensor for human-motion detection and a human–machine interface. Journal of Materials Chemistry C. 2022; 10(41): 15554-15564. doi: 10.1039/d2tc03147g

13. Rodriguez-Labra JI, Kosik C, Maddipatla D, et al. Development of a PPG Sensor Array as a Wearable Device for Monitoring Cardiovascular Metrics. IEEE Sensors Journal. 2021; 21(23): 26320-26327. doi: 10.1109/jsen.2021.3064219

14. Wang L, Wang D, Wang K, et al. Biocompatible MXene/Chitosan-Based Flexible Bimodal Devices for Real-Time Pulse and Respiratory Rate Monitoring. ACS Materials Letters. 2021; 3(7): 921-929. doi: 10.1021/acsmaterialslett.1c00246

15. Yao N, Wang X, Ma S, et al. Single optical microfiber enabled tactile sensor for simultaneous temperature and pressure measurement. Photonics Research. 2022; 10(9): 2040. doi: 10.1364/prj.461182

16. Xu B, Ye F, Chen R, et al. A wide sensing range and high sensitivity flexible strain sensor based on carbon nanotubes and MXene. Ceramics International. 2022; 48(7): 10220-10226. doi: 10.1016/j.ceramint.2021.12.235

17. Shen Y, Yang W, Hu F, et al. Ultrasensitive wearable strain sensor for promising application in cardiac rehabilitation. Advanced Composites and Hybrid Materials. 2022; 6(1). doi: 10.1007/s42114-022-00610-3

18. Xu H, Gao L, Zhao H, et al. Stretchable and anti-impact iontronic pressure sensor with an ultrabroad linear range for biophysical monitoring and deep learning-aided knee rehabilitation. Microsystems & Nanoengineering. 2021; 7(1). doi: 10.1038/s41378-021-00318-2

19. Peng Y, Zhou J, Song X, et al. A Flexible Pressure Sensor with Ink Printed Porous Graphene for Continuous Cardiovascular Status Monitoring. Sensors. 2021; 21(2): 485. doi: 10.3390/s21020485

20. Lozano Montero K, Laurila MM, Peltokangas M, et al. Self-Powered, Ultrathin, and Transparent Printed Pressure Sensor for Biosignal Monitoring. ACS Applied Electronic Materials. 2021; 3(10): 4362-4375. doi: 10.1021/acsaelm.1c00540